International Tables for Crystallography (2006). Vol. C, Section 2.3.1.2, pp. 50–52.

2.3.1.1.7. *Axial divergence*

Divergence in the axial direction (formerly also called 'vertical divergence') causes asymmetric broadening and shifts the reflections. The aberration is illustrated in Fig. 2.3.1.11 for a low-2θ reflection in the transmission-specimen mode (Subsection 2.3.1.2). The narrow profile was obtained with $\delta = 4.4^\circ$ parallel slits placed between the monochromator and detector, and the broad profile with the slits removed. The slits caused a 33% reduction in peak intensity. This problem was recognized in the first design of the diffractometer using the X-ray tube line focus when parallel slits were used in the incident and diffracted beams to limit the effect (Parrish, 1949). Increasing the radius reduces the effect if the slit length is kept constant. The intensity is also reduced because the chord length intercepted is a smaller fraction of the longer radius diffraction cone. The construction of parallel (Soller) slits (Soller, 1924) is shown in Fig. 2.3.1.5(*d*).

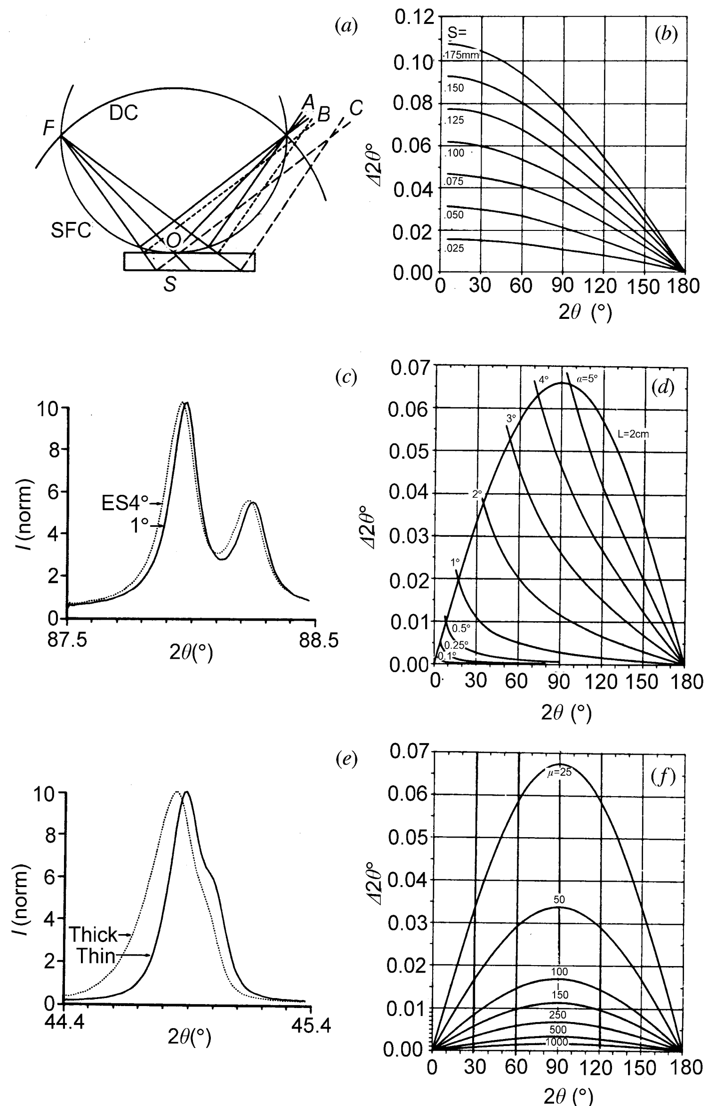

Fig. 2.3.1.10. (*a*) Origin of specimen-related aberrations in focusing plane of conventional reflection specimen diffractometer (Fig. 2.3.1.3). *A* no aberration from curved specimen; *B* flat specimen; *C* specimen displacement from 0. (*b*) Computed angular shifts caused by specimen displacement, $R = 185$ mm. (*c*) Flat-specimen asymmetric aberration, Si(422), Cu $K\alpha_1$, $K\alpha_2$ peak intensities normalized. (*d*) Computed flat-specimen centroid shifts for various apertures; parabola for constant irradiated 2 cm specimen length. (*e*) Transparency asymmetric aberration, LiF(200) powder reflection, Cu $K\alpha$, peak intensities normalized, thin specimen (solid-line profile) 0.1 mm thick; thick specimen (dotted-line profile) 1.0 mm, α_{ES} 1°, α_{RS} 0.046°. (*f*) Computed transparency centroid shifts for various values of linear absorption coefficient.

The calculation of the aberration and the present status is summarized by Wilson (1963, pp. 40–45). The results depend on the aperture of the parallel slits, the length of the entrance and receiving slits, and 2θ. In the limit of small s, the shift of the centroid is

$$\Delta(2\theta, \text{rad}) = (s/l)^2 \cot 2\theta/6, \qquad (2.3.1.15)$$

where s is the spacing and l the length of the foils. The shift becomes very large at small 2θ's but not infinite as equation (2.3.1.15) implies. The shift is to smaller 2θ's in the forward-reflection region and to larger 2θ's in back-reflection. However, the mathematical formulation is difficult to quantify because in the forward-reflection region the axial divergence convolves with the flat-specimen aberration to increase the asymmetry. In the back-reflection region, the effect is not so obvious because the distortion is smaller and the Lorentz and dispersion factors also stretch the profiles to higher angles.

2.3.1.1.8. *Combined aberrations*

Additional aberrations are caused by inaccurate instrument set-up and alignment. For example, if the receiving-slit position is incorrect, the profiles are broadened. If, in addition, the incident beam is mis-centred or the θ–2θ is incorrect, a peak shift accompanies the broadening because the aberrations convolute, causing larger distortions and peak shifts than the individual aberrations, for example, flat-specimen, transparency, and axial divergence.

2.3.1.2. *Transmission specimen, θ–2θ scan*

Transmission-specimen methods are not as widely used as reflection methods but they provide important supplemental data and have advantages in a number of applications. Reflections occur from lattice planes oriented normal to the specimen surface rather than parallel. Reflection and transmission patterns can be compared to determine texture and preferred-orientation effects. The transmission method is better suited to the measurement of large d's. Smaller specimen volumes are required. The surface 'roughness' which may cause large intensity errors due to the microabsorption in reflection specimens is largely reduced.

The same basic diffractometer is used for both methods but the geometry is different because the diffracted beam continues to

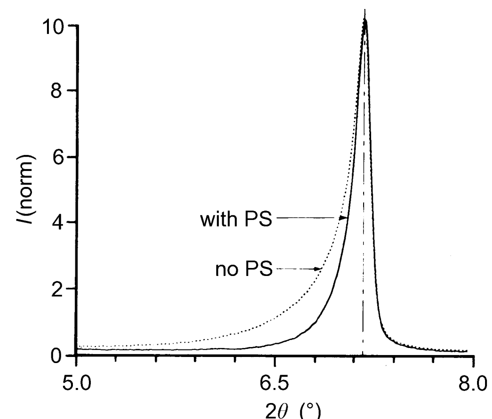

Fig. 2.3.1.11. Effect of axial divergence on profile shape. Narrow profile recorded with parallel slits (PS), $\delta = 4.4^\circ$ between monochromator and detector Fig. (2.3.1.12), and broad profile with these parallel slits removed. Faujasite, Cu $K\alpha$, α_{ES} 2°.

Copyright © 2006 International Union of Crystallography

diverge after it passes through the specimen and the monochromator is required to refocus the beam, on the detector as shown in Fig. 2.3.1.12 (de Wolff, 1968*b*; Parrish, 1958). The monochromator can be placed before or after the specimen and the position has different effects on the pattern. Using the monochromator in the diffracted beam, the intensity and width of the profiles are determined by the X-ray focal line width and the quality of the bent monochromator rather than the receiving slit which serves as an antiscatter slit. This geometrical arrangement places the virtual image VI of the focal line at the intersection of the focusing circles. After reflection from the specimen, the divergent beam is again reflected by the focusing crystal M and converges on the detector. The pattern is recorded with θ–2θ scanning with the monochromator and detector both mounted on a rigid arm rotating around the diffractometer axis. A beam stop MS can be translated and moved in and out near the crossover point to prevent the primary beam from entering the detector at small 2θ's. To avoid long radii, the crystal surface is cut at an angle σ (about 3°) to the reflecting lattice plane. The distances are related by

$$\begin{aligned}(l_1 + l_2)/l_3 &= [\sin(\theta_M + \sigma)]/[\sin(\theta_M - \sigma)]\\ R_{\rm FC} &= [l_1 + l_2]/[2\sin(\theta_M + \sigma)]\\ &= l_3/[2\sin(\theta_M - \sigma)],\end{aligned} \qquad (2.3.1.16)$$

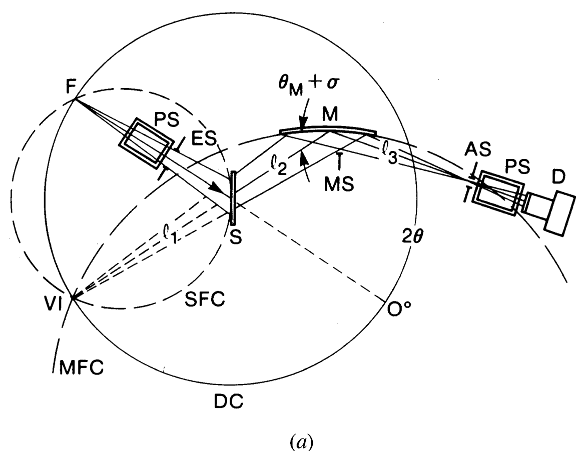

(*a*)

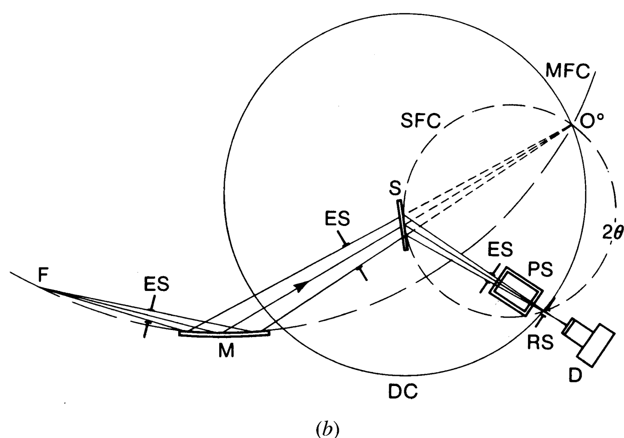

(*b*)

Fig. 2.3.1.12. X-ray optics of the transmission specimen with asymmetric focusing monochromator and θ–2θ scanning. (*a*) Monochromator in diffracted beam. θ_M Bragg angle of monochromator with surface cut at angle σ to reflecting plane, MS adjustable beam stop, l_1, l_2, and l_3 defined in text and other symbols listed in Fig. 2.3.1.3. (*b*) Monochromator in incident beam, equivalent to Guinier focusing camera.

where θ_M is the Bragg angle of the monochromator for the selected wavelength and the l's are shown in Fig. 2.3.2.12(*a*).

Because the profile shape and the intensity are determined by the monochromator, the crystal quality and the accuracy of the bending are crucial factors in determining the quality of the pattern. A flat thin quartz (101) wafer bent with a special device to approximate a section of a logarithmic spiral has been successfully used (de Wolff, 1968*b*). The curvature can be varied to obtain the sharpest focus. Thin silicon crystals that can be bent are now available, and Johann and Johannsen asymmetric crystals may be used. Pyrolytic graphite monochromators are not applicable; the radii would be longer because graphite is too soft to be cut at an angle, and a receiving slit would be necessary to define the diffracted beam because the monochromator produces a broad reflection.

A polarization factor is introduced by the monochromator,

$$p = (1 + k\cos^2 2\theta)/(1 + k), \qquad (2.3.1.17)$$

where $k = \cos^2 2\theta_M$ for mosaic crystals and $k = \cos 2\theta_M$ for perfect crystals. The value of k is strongly dependent on the surface finish of the crystal and the crystal should be measured to determine the effect. A specimen with accurately known structure factors such as silicon can be used to calibrate the intensities.

The $K\alpha$-doublet separation is zero at the 2θ angle at which the dispersion of the specimen compensates that of the monochromator, *i.e.* the 2θ at which the monochromator is aligned and also depends on the distances. The $K\alpha_1$ and $K\alpha_2$ peaks are superposed and appear as a single peak over a small range of 2θ's. The $K\alpha_2$ peak gradually separates with increasing 2θ but the separation is less than calculated from the wavelengths and the intensity ratio may not be 2:1 until higher angles are reached as shown in Fig. 2.3.1.8.

A larger angular aperture α_T can be used for transmission than for reflection α_R because the specimen is more nearly normal to than parallel to the primary beam:

$$\alpha_T/\alpha_R = 2R_D/[1 + (R/l_2)L_s], \qquad (2.3.1.18)$$

where the diffractometer radius $R_D = l_1$. For $R_D = 170$ mm, specimen length $L_S = 20$ mm and $l_2 = 65$ mm; α_T could be 4.7 times larger than α_R but the monochromator length usually limits it to about 3°. The smallest reflection angle that can be measured is

$$2\theta_{\rm min} = \alpha_T[(R_D + l_2)/l_2]. \qquad (2.3.1.19)$$

Using $\alpha_T = 0.5°$, $2\theta_{\rm min} = 1.75°$ and $d = 50$ Å for Cu $K\alpha$ radiation.

Specimen preparation is not difficult and the preparation can be easily tested and changed. The specimen must be X-ray transparent and can be a free-standing film or foil, or a powder cemented to a thin substrate. The substrate selection is important because its pattern is included. If both transmission and reflection patterns are to be compared, the substrate should be selected to have a minimal contribution to both. For example, Mylar is a good substrate for transmission but has a strong reflection pattern, and although rolled Be foil has a few reflections it is often satisfactory for both.

The absorption factor is

$$A = (t/\cos\theta)\exp(-s/\cos\theta), \qquad (2.3.1.20)$$

where t is the powder thickness and s is the sum of the products of the absorption coefficients and thicknesses of the powder and the substrate. The optimum specimen thickness to give the highest intensity is $\mu t = 1$, *i.e.* the specimen should transmit about 38% of the incident $K\alpha$ intensity. The transmission can be

easily measured with a standard specimen set to reflect the $K\alpha$ and the specimen to be measured inserted normal to the diffracted beam in front of the detector. It is not critical to achieve the exact value and a range of ±15–20% of the transmission can be tolerated. This minimizes the effect of the absorption change with 2θ, and corrections of the relative intensities are required only when accurate values are required.

The intensity of the incident beam can be measured at 0° in the same geometry and used to scale the relative intensities to 'absolute' values. The flat specimen, transparency, and specimen surface displacement aberrations are similar to those in reflection specimen geometry except that they vary as $\sin\theta$ rather than $\cos\theta$. This is an important factor in the measurement of large-d-spacing reflections. The flat-specimen effect is smaller because the irradiated specimen length is usually smaller. The transparency error is also usually smaller because thin specimens are used.

An important advantage of the method is that the specimen displacement can be directly determined by measuring the peak in the normal position and again after rotating the specimen holder 180°. The correct peak position is at one-half the angle between the two values. The axial divergence has the same effect as in reflection. The limitations are that only the forward-reflection region is accessible, and the intensity is about one-half of the reflection method (except at small angles) because smaller specimen volumes are used.

An alternative arrangement for the transmission specimen mode is to use an incident-beam monochromator as shown in Fig. 2.3.1.12(*b*). This is similar to the geometry used in the Guinier powder camera with the detector replacing the film. A high-quality focusing crystal is required. Wölfel (1981) used a symmetrical focusing monochromator with 260 mm focal length for quantitative analysis. Göbel (1982) used an asymmetric monochromator with a position-sensitive detector for high-speed scanning, see §2.3.5.4.1. By proper selection of the source size and distances, the $K\alpha_2$ can be eliminated and the pattern contains only the $K\alpha_1$ peaks (Guinier & Sébilleau, 1952). This geometry can have high resolution with the FWHM typically about 0.05 to 0.07°. The profile widths are narrower for the subtractive setting of the monochromator than for the additive setting.

The pattern is recorded with θ–2θ scanning. The 0° position can be determined by measuring 4θ, *i.e.* peaks above and below 0°, or calibration can be made with a standard specimen. A slit after the monochromator limits the size of the beam striking the specimen. The width and intensity of the powder reflections are limited by the receiving-slit width. A parallel slit is used between the specimen and detector to limit axial divergence.

The full spectrum from the X-ray tube strikes the monochromator and only the monochromatic beam reaches the specimen, so that it is preferred for radiation-sensitive materials. On the other hand, the radiation reaching the specimen may cause fluorescence (though considerably less than the full spectrum) which adds to the background.

2.3.1.3. *Seemann–Bohlin method*

The Seemann–Bohlin (*S–B*) diffractometer has the specimen mounted on a radial arm instead of the axis of rotation and a linkage or servomechanism moves the detector around the circumference of a fixed-radius focusing circle while keeping it pointed to the stationary specimen. All reflections occur simultaneously focused on the focusing circle as shown in Fig. 2.3.1.13(*a*). The method was originally developed for powder cameras by Seemann (1919) and Bohlin (1920) but was not widely used because of the limited angular range and the broad reflections caused by inclination of the rays to the film. The diffractometer eliminates the broadening and extends the angular range. Diffractometers designed for this geometry have been described by Wassermann & Wiewiorosky (1953), Segmüller (1957), Kunze (1964*a*,*b*), Parrish, Mack & Vajda (1967), King, Gillham & Huggins (1970), Feder & Berry (1970), and others.

The geometry is shown in Fig. 2.3.1.13(*b*) (Parrish & Mack, 1967). Reflections occur from lattice planes with varying inclinations β_H to the specimen surface. The reflecting position of a plane H is $\theta_H = \gamma + \beta_H$, where γ is the incidence angle and $4\theta_H$ the reflection angle. The maximum value of β_H is about 45°. It is essential to align the specimen tangent to FC. This is a critical adjustment because even a small misalignment causes profile broadening and loss of peak intensity.

The source may be the line focus of the X-ray tube [F in Fig. 2.3.1.13(*b*)] or at the focus of a monochromator [ES in Fig. 2.3.1.13(*a*)]; in the latter case, the entrance slit at F' limits the divergent beam reaching the specimen. The source, specimen centre O, and receiving slit RS lie on the specimen focusing circle SFC, which has a fixed radius r. The incidence angle γ is given by

$$\gamma = \arcsin(b/2r), \qquad (2.3.1.21)$$

where b is the distance from F or F' to O, or $2r\sin\gamma$. The γ angle determines the angular range that can be recorded with a given r, decreasing γ decreases $2\theta_{\min}$. The relationships of specimen position on the focusing circle and the recording range

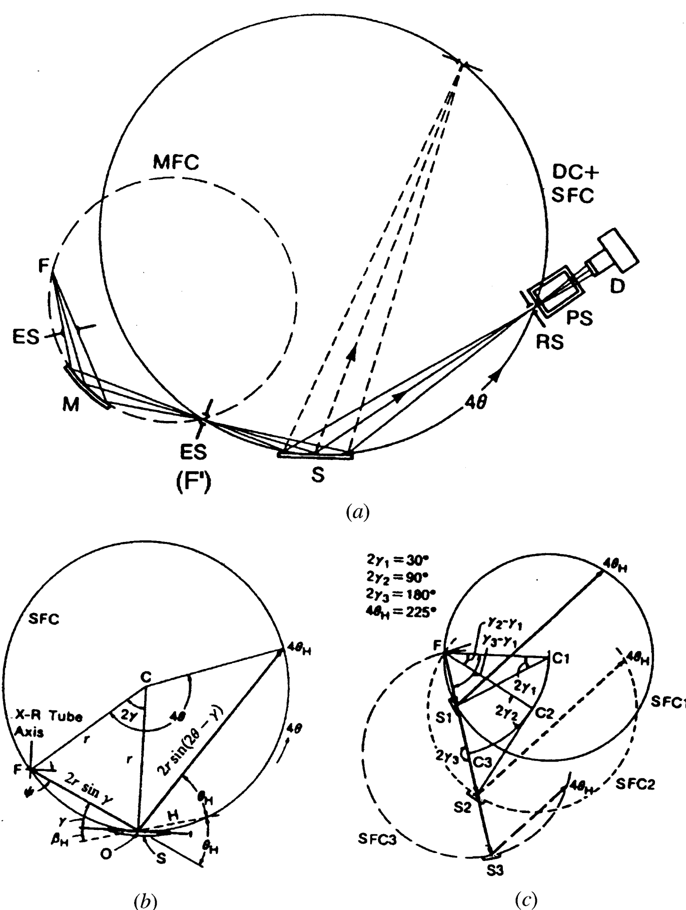

Fig. 2.3.1.13. Seemann–Bohlin method. (*a*) X-ray optics using incident-beam monochromator. (*b*) X-ray tube line-focus source showing geometrical relations: γ mean angle of incident beam, β_H inclination of reflecting plane H to specimen surface, θ_H Bragg angle of H plane, t tangent to focusing circle at O. (*c*) Diffractometer settings for various angular ranges.

references